Molecular dynamics study on water desalination through functionalized nanoporous graphene

Article · January 2017

DOI: 10.1016/j.carbon.2017.01.099

5 authors, including:

Zhongjin He
National University of Singapore
8 PUBLICATIONS **76** CITATIONS
SEE PROFILE

Krishna Mohan Gupta
National University of Singapore
18 PUBLICATIONS **201** CITATIONS
SEE PROFILE

Ruifeng Lu
Nanjing University of Science and Technology
97 PUBLICATIONS **1,084** CITATIONS
SEE PROFILE

Carbon 116 (2017) 120–127

Contents lists available at ScienceDirect

Carbon

journal homepage: www.elsevier.com/locate/carbon

Molecular dynamics study on water desalination through functionalized nanoporous graphene

Yunhui Wang [a, b, c], Zhongjin He [b], Krishna M. Gupta [b, **], Qi Shi [a, b], Ruifeng Lu [a, *]

[a] Department of Applied Physics, Nanjing University of Science and Technology, Nanjing 210094, PR China
[b] Department of Chemical and Biomolecular Engineering, National University of Singapore, 117576, Singapore
[c] Information Physics Research Center, School of Science, Nanjing University of Posts and Telecommunications, Nanjing 210023, PR China

ARTICLE INFO

Article history:
Received 21 September 2016
Received in revised form
31 December 2016
Accepted 28 January 2017
Available online 31 January 2017

ABSTRACT

Molecular dynamics simulations were employed to investigate water desalination through functionalized nanoporous graphene membranes. Six graphene membranes were considered in which the carbon atoms of the pores were terminated by hydrogen or hydroxyl functional groups. The results demonstrate that water desalination occurs under external pressure and water flux permeating the membranes scales linearly with external pressure and pore diameter. The hierarchy of water flux through the functionalized graphene membranes was explained by potential of mean force. The salt rejection from smallest pore was 100% and decreases as pore diameter increases. Both Na^+ and Cl^- ions permeate through membrane with the largest pore, and the selectivity of the ions permeating exhibits a significant correlation with functional group. The designed graphene membrane shows excellent performance in terms of both salt rejection and water transport. Ultrahigh water permeance of 785.6 L per $m^2 \cdot h \cdot bar$ obtained is two or three orders of magnitude higher than current commercially available reverse osmosis (RO) and nanofiltration membranes. This simulation study provides a microscopic insight into water desalination in various functionalized graphene membranes and reveals governing factor for water flux and also suggests a potential candidate as a RO membrane.

1. Introduction

Recent water crisis has attracted much attention in the globe owing to the rapid growth of world population, accelerated industrialization and environmental pollution [1–6]. Desalination is known to be one of the most promising sustainable approaches for water treatment to supply fresh water. Currently, reverse osmosis (RO) membranes have been prevalent in commercial desalination systems worldwide mainly due to its energy-efficiency, flexible installation, high-resistant and lower cost.

As membrane materials play a key role in desalination performance, carbon structures with various dimensionality such as carbon nanotubes (CNTs) [7–18], graphene [19–31] and covalent triazine frameworks (CTFs) [32–34] as well as metal organic frameworks (MOF) [35–38] have been previously investigated as promising membranes. Although CNTs are expected to possess high water permeability and exhibit a high salt rejection, it is currently difficult to fabricate well aligned and high density CNTs with large lengths [39,40]. Despite the three dimensional networks of zeolites that can effectively reject salt ions, the water permeability is low [35,36]. Furthermore, the CTFs [34] possess a high water permeance of 64.2 $L \cdot cm^{-2} \cdot day^{-1} \cdot MPa^{-1}$ similar to graphene (66 $L \cdot cm^{-2} \cdot day^{-1} \cdot MPa^{-1}$) [19], however, the salt rejection is lower than graphene. To search a potential membrane for desalination, we should consider overall performance in terms of both permeance and salt rejection.

Recently, with the development of experimental technologies, large-area graphene nano sheets have been successfully prepared [41]. In such a two dimensional sheet of sp^2-bonded carbon atoms forming a hexagonal honeycomb lattice, the delocalized electron clouds of π-orbitals take up the voids of aromatic rings in graphene sheet, which is able to prevent the permeation of even atomic helium [42,43]. Nevertheless, heavy ions were reported to bombard monolayer graphene film and produce operated nanopores, which have been more commonly known as nanoporous graphene [44]. Existing studies have already found potential applications of nanoporous graphene in fields such as gas separation [45–56] and

* Corresponding author.
** Corresponding author.
E-mail addresses: chekmg@nus.edu.sg (K.M. Gupta), rflu@njust.edu.cn (R. Lu).

http://dx.doi.org/10.1016/j.carbon.2017.01.099
0008-6223/

DNA sequencing [57–61]. Generally, functionalization of pores is associated with the formation of sp^3 carbon network structure through the rehybridization of existing one or more sp^2 carbon atoms accompanied by simultaneous loss of electronic conjugation [28,62]. The functionalizations of nanoporous graphene sheets with various active groups and inorganic nano particles make the properties of the pristine graphene to be engineered as a class of new and exciting materials for specific applications, such as desalination. As is well known, the water flux varies inversely with membrane thickness, so the exfoliated graphene as single atomic layer membrane could be promising for desalination. The first attempt to investigate functionalized graphene as desalination membrane was reported by Cohen-Tanugi and Grossman [19] using molecular dynamics (MD) simulations. They demonstrated that the functionalized nanoporous graphene membranes could perform more than 99% salt rejection and provide water permeance up to 66 $L \cdot cm^{-2} \cdot day^{-1} \cdot MPa^{-1}$ which is 2–3 orders of magnitude higher than that of current commercially available RO membranes and nanofiltration membranes [63]. Therefore, there is a large opportunity to further explore functionalized graphene materials for excellent desalination performance.

In this work, we have performed MD simulations for seawater desalination by further considering three types of nanoporous graphene membranes with hydrogenated (-H) and hydroxylated (-OH) terminations. Thus, the role of pore sizes and pore functionalization under induced pressure can be exclusively revealed. Following this introduction, the models and methods used are briefly described in Section2. In Section 3, salt rejection and water permeance through the graphene membranes are presented and compared with other membranes. Finally, the concluding remarks are summarized in Section 4.

2. Models and methods

Fig. 1 shows the atomistic structure of three types of graphene nanopores. It is clear that the nanoporous graphene membranes are different in terms of pore size and chemical functional group. Two different functionalized nanopores named hydrogenated pore (P_H pore) and hydroxylated pore (P_OH pore) were used in this work. For practical purposes of the real liquid, hydrogen bonds will be formed if the separation of the oxygen atoms on neighboring water molecules is less than 3.5 Å, and about 3.58 hydrogen bonds per water molecule are obtained at ambient conditions [64]. Thus, the diameter of the water molecular cluster is about 5.0–6.5 Å. On the other hand, to effectively reject ion transport across graphene membrane, the pore diameters should be chosen to be similar or smaller than the diameters of hydrated Na^+ and Cl^- ions which are 6.4 and 7.7 Å respectively [65]. Because the pore diameter plays a key role in governing water transport through the nanoporous graphene membrane, the pore diameters are appropriately chosen as 8.2, 5.6, 5.2, 6.6, 4.6 and 3.8 Å for membranes of Fig. 1(a)–(f), respectively. In-plane dimensions of the functionalized nanoporous graphene membranes are 29.8 × 29.5 $Å^2$ with a pore density of 1.1×10^{13} cm^{-2}.

Water desalination through each graphene membrane was simulated in a system schematically illustrated in Fig. 2. The membrane was located at the center of a simulation box at 30 Å since simulation box length is 60 Å along z dimension. The simulation box was filled with 0.5 mol/L NaCl aqueous solution, corresponding to a salt concentration of 33 g/L which is slightly lower than seawater of 35 g/L. Each system was initially subjected to energy minimization using the steepest descent method, then velocities were assigned according to the Maxwell-Boltzmann distribution at 300 K. Finally,

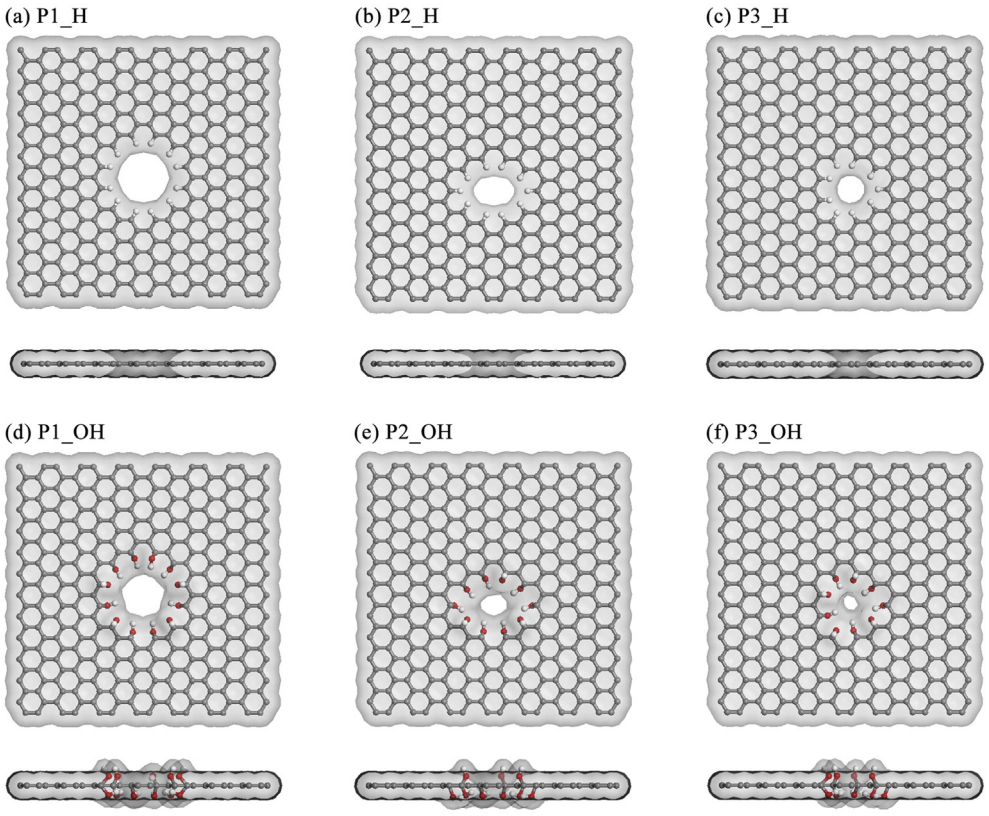

Fig. 1. Functionalized pores in graphene membranes: (a) P1_H pore, (b) P2_H pore, (c) P3_H pore, (d) P1_OH pore, (e) P2_OH pore, and (f) P3_OH pore. (A colour version of this figure can be viewed online.)

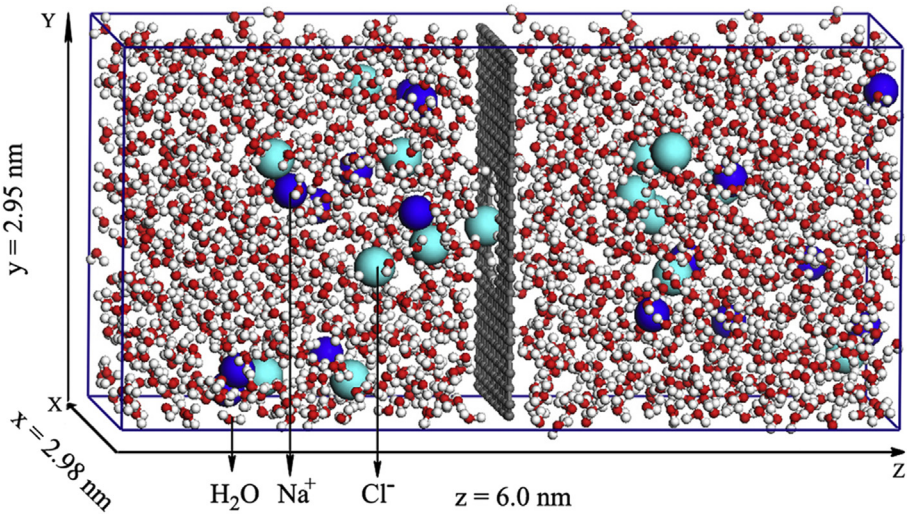

Fig. 2. Schematic diagram of simulation cell for P1_H pore system. (A colour version of this figure can be viewed online.)

non-equilibration molecular dynamics (MD) simulation was conducted at 298 K. For all runs, the functionalized graphene membrane was held flexible except the carbon atoms at the edge of the graphene sheet, meanwhile, the water, Na^+ and Cl^- ions were allowed to move freely during the MD simulations. The effective potential energy of intermolecular interactions is given by the sum of Lennard–Jones (LJ) and Coulomb potentials for long range and short range interactions, respectively, following the expression: $U_{\text{nonbond}} = \sum 4\varepsilon_{ij}\left[\left(\frac{\sigma_{ij}}{r_{ij}}\right)^{12} - \left(\frac{\sigma_{ij}}{r_{ij}}\right)^{6}\right] + \sum \frac{q_i q_j}{4\pi\varepsilon_0 r_{ij}}$, where r_{ij} refers to the distance between atoms i and j, ε_{ij} and σ_{ij} represent the LJ parameters, and q_i and q_j represent the partial charge assigned to atoms i and j, respectively. A cutoff of 14 Å was used to calculate the LJ interactions, and the particle-mesh Ewald method was used to evaluate the electrostatic interactions with grid spacing of 1.2 Å and real-space cutoff of 14 Å.

All simulations were performed using GROMACS 5.0.4 software [66]. The MD simulations were implemented in the NVT canonical ensemble with the total time of 30 ns and the periodic boundary conditions were imposed in all directions. To create a pressure drop across the graphene in the form of hydrostatic pressure, external forces were applied to all the water molecules [67], which have been also applied to investigate Poiseuille flow [68], where the constant field acts in the same way as a gravitational force. However, in such simulations the energy added to the system by the external force is dissipated thermally through the walls in order to perturb the dynamics of the fluid as little as possible. This is achieved by applying a thermostat to the wall particles only, rather than the fluid. The methods of thermostating fluids in simulations involving flows have been discussed previously [69] which concludes that thermostating the fluid directly will alter the dynamics of the fluid. It should also be noted that even when applying a Nosé-Hoover thermostat in the case of a system undergoing a net flow, the streaming velocity of the particles should be taken into account when calculating the temperature, although this effect may be small. A more reasonable way is to apply a force to water in a thin slab with a suitable distance away from the membrane, which has been employed in other works [70–73].

The method used here is commonly employed for pressure driven flow [74,75]. Recently, Richard et al. [76] compared the method by using a graphene sheet as a rigid piston to exert external pressure with the method of applying external pressure in present work. They found that no significant difference was observed between different methods. Thus, we hope the water permeability will not be affected by choosing the method in this work. Then, the water gradient can be performed in MD simulations by applying a constant force F in the z-direction on one water molecule, which is given by $F = \Delta P \cdot A/n$, where ΔP is the chosen pressure, A is the membrane area, n is the total number of water molecules in the box. In our simulations, the pressure was selected in the range of 10–200 MPa. Water was modeled using the TIP3P potential [77], and the short-range interactions for atomic species were modeled by the LJ potential and Coulombic terms. All the parameters employed in this desalination system for all the interaction types are summarized in Table S1 (supplementary materials). The partial charges and LJ parameters used for the functionalized graphene membrane and Na^+, Cl^- were taken from the CHARMM27 [78] and AMBER03 [79] force fields, respectively.

3. Results and discussion

We first studied the number of water molecules N_w filtered by graphene membranes as a function of time with pressure ranges from 10 to 200 MPa. It can be seen from Fig. 3 that N_w increases almost linearly with time despite small fluctuations due to the random thermal motion of water molecules. The linear curves indicate that water molecules permeate across the membrane at a relatively constant rate. Moreover, higher the pressure, larger the N_w. As we shall see below, the diameter and the functional group of nanopores play a key role in governing water transport through the graphene membrane. The radius of -H group is smaller than -OH, thus the pore size of hydrogenated membrane is a little larger than that hydroxylated membrane for the same pore. However, the hydrophobic and hydrophilic properties also affect the desalination. For small diameter, the water molecule goes through the pore modified with hydrophilic functional group easier than the hydrophobic pore. More specifically, N_w across the hydrogenated membrane is higher than that hydroxylated one as shown in Fig. 3(a) for P1 at the same given pressure. The hydrophobic pore (-H functional) possessing higher N_w compared to hydrophilic (-OH functional) is due to the dominance of size effect over functionality specially for large pore P1. This is because the pore size of P1 membrane is much larger than the water molecule. Nevertheless, N_w of the hydrogenated membrane is smaller than that from hydroxylated membrane for graphene layers with P2 (Fig. 3(b)) and

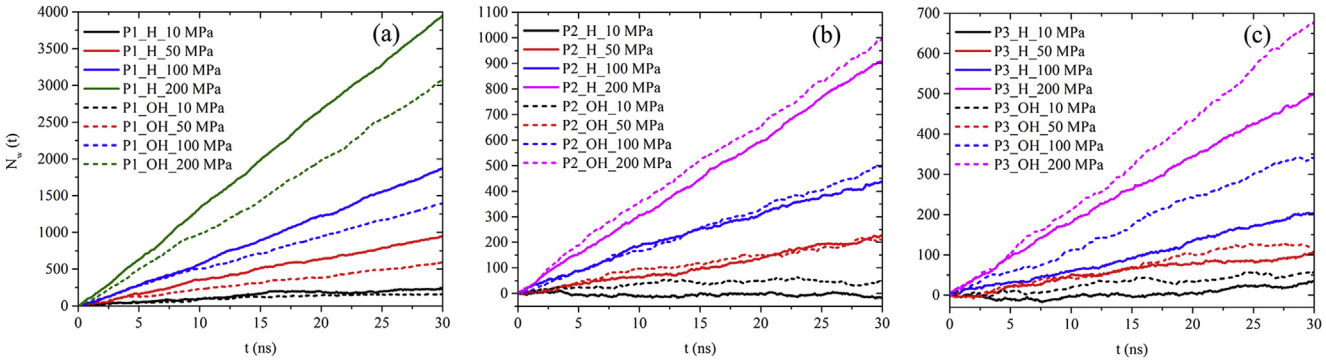

Fig. 3. The number of water molecules passing through the (a) P1_H and P1_OH pores, (b) P2_H and P2_OH pores and (c) P3_H and P3_OH pores at the pressures of 10, 50, 100 and 200 MPa. (A colour version of this figure can be viewed online.)

P3 (Fig. 3(c)) pores at the same given pressure, indicating that the functionalized group plays an important role for a relatively small pores. On the basis of N_w as a function of time t, the water fluxes permeating across the hydrogenated and hydroxylated pores of nanoporous graphene membranes are calculated and tabulated in Fig. 4. The hierarchy of fluxes is the same as N_w (Fig. 3). Following the trend of pore size as P1 < P2 < P3, both N_w and water flux decrease in the same order. Obviously, with larger pore P1 than P2 and P3, both N_w and water flux are much higher.

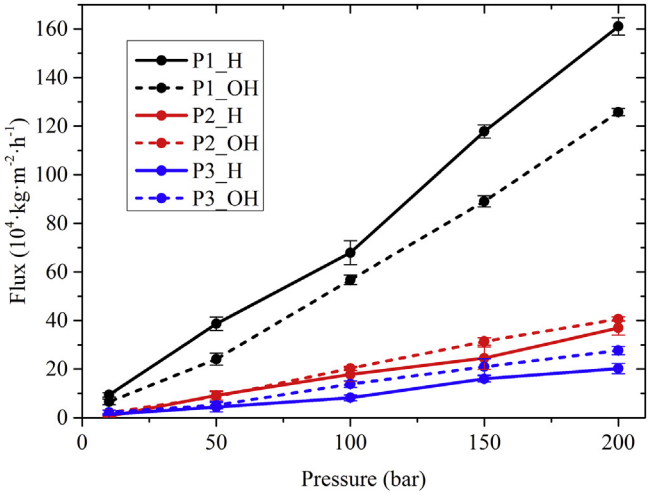

Fig. 4. Water flux in six graphene membranes at the pressures of 10, 50, 100 and 200 MPa. (A colour version of this figure can be viewed online.)

To judge the performance of the graphene membranes, it is desirable to analyze the slat rejection in addition to water flux. Keep in mind that the diameters of the Na^+ and Cl^- are about 2.0 Å and 3.6 Å, respectively, which are larger than the smallest pore size of the studied membrane. However, both Na^+ and Cl^- are not found to cross through P2 and P3 pores. It is because that the water molecules will be gathered around the Na^+ and Cl^- ions and form hydrated structures by means of hydrogen bonds. The average number of water molecules for hydration is about 5.2–7.1 in the first hydration shell around the Na^+ and Cl^- ions [80]. Thus, the diameters of the hydration structures for Na^+ and Cl^- ions are larger than the P2 and P3 pores. Nevertheless, ions are able to pass through larger pore P1. Fig. 5 shows the number of Na^+ and Cl^- ions across the large P1_H and P1_OH pores of graphene membranes. With increasing pressure, both Na^+ and Cl^- ions flow increase, while the ion permeation rates are quite difference for hydrogenated and hydroxylated membranes. In Fig. 5(a), almost no Cl^- ions can penetrate the P1_OH pore of graphene membrane, but they can pass through the P1_H pore of graphene membrane due to the positively charged hydrogen functional groups. Analogously in Fig. 5(b), Na^+ ions can go through P1_OH pore more smoothly than that in the P1_H because the hydroxyl functional groups carry the negative charge. In 2008, Sint and coworkers showed computationally that

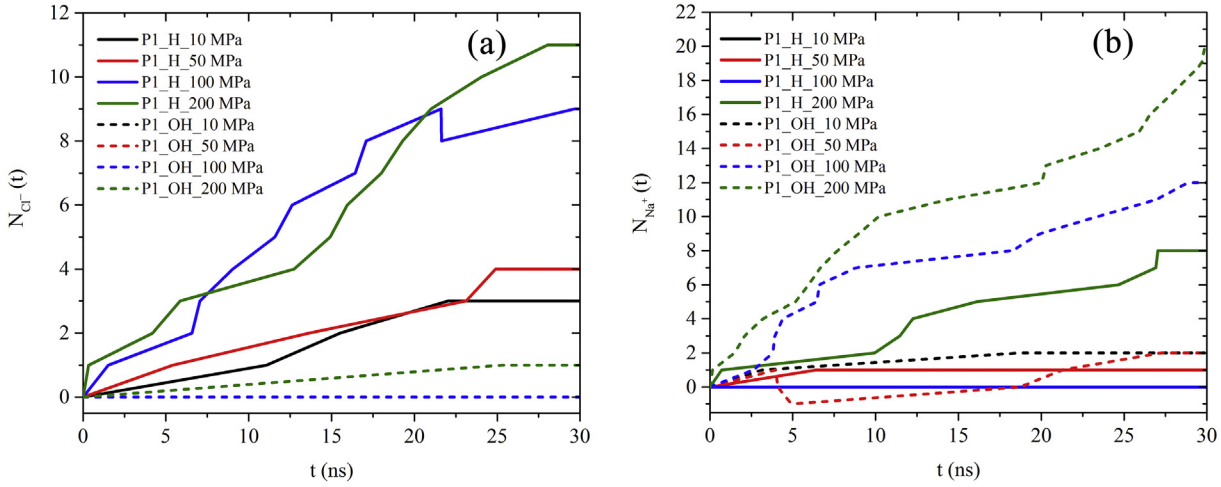

Fig. 5. The number of Cl^- and Na^+ passing through the P1_H pore and P1_OH pore at the pressures of 10, 50, 100 and 200 MPa. (A colour version of this figure can be viewed online.)

graphene was selectively permeable to certain solvated ions and impermeable to others when nano sized pores exist in the membrane [81]. The authors claimed that the chemical functional groups at the edge of the nanopores play a key role in determining ion rejection, which is in consistent with our finding.

To quantitatively characterize the motion of the water molecules, Fig. 6 presents the density distributions along the *z*-direction. As time lapses, the density distribution curves of water shift from left side to right side under induced pressure, which is consistent with the direction of the applied pressure. Around $z = 3$ nm, there is a minima in density profile that is corresponding to position of graphene membrane. A large number of water molecules stay in the left side of the graphene membrane under induced pressure, therefore, the density distribution curve of the water in the left side is higher than that in the right side. Moreover, upon increasing the pressure from 10 to 200 MPa, water molecules move faster and faster along the *z*-direction, thus the density in the left side is increased with increasing pressure, and the opposite trend can be observed in the right side because the passed water molecules move away to the membrane quickly under the induced pressure. Meanwhile, by comparing Fig. 6(a) with (b), it can be seen that the density on the left side in the former is larger than that in the latter under same applied pressure. This is due to the hydrophilic nature of the hydroxyl group in the P1_OH in contrast to the hydrophobic nature in P1_H membrane. The similar behavior can also be observed through other graphene membranes (Fig. S1).

In order to shed light on the penetration mechanism across the functionalized nanoporous graphene, the potential of mean force (PMF) which is the free energy profile of a water molecule passing through the membrane was calculated. The PMF of one water molecule passing through the graphene membrane under equilibrium conditions was determined using Boltzmann sampling. The energetic barriers for water molecules at different positions along ***z*** direction were calculated by $F(r) = -RTln[\rho(r)]$, where R is the gas constant, T is the temperature and $\rho(r)$ is the density at position r. The method is a quick way to calculate the free energy profiles and frequently used in other works [82–84]. Please note that another way is to use umbrella sampling to calculate PMF in the equilibrium state [22], however, it is also not for non-equilibrium systems. Firstly, we figure out the PMF for graphene membranes with the hydrogenated and hydroxylated P1, P2 and P3 pores at the pressure of 50 MPa as shown in Fig. S2. Obviously, there is an energy barrier faced for water molecules to penetrate the membrane ($z = 3$ nm). It is well known that smaller the energy barrier, easily molecules go

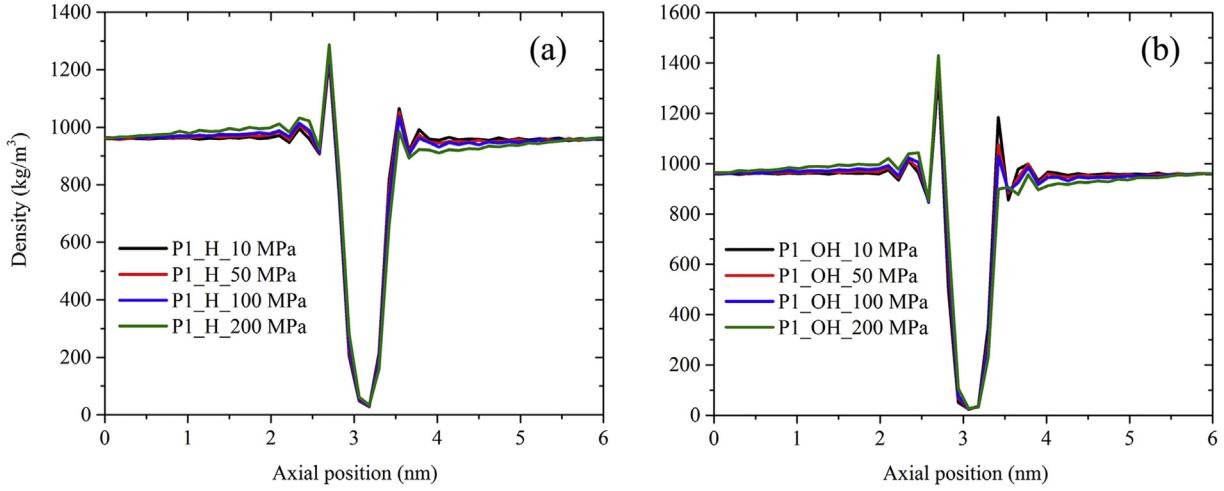

Fig. 6. Density profiles of water in the *z*-direction of the system for the (a) P1_H pore and (2) P1_OH pore at the pressures of 10, 50, 100 and 200 MPa in the time stage of 29–30 ns. (A colour version of this figure can be viewed online.)

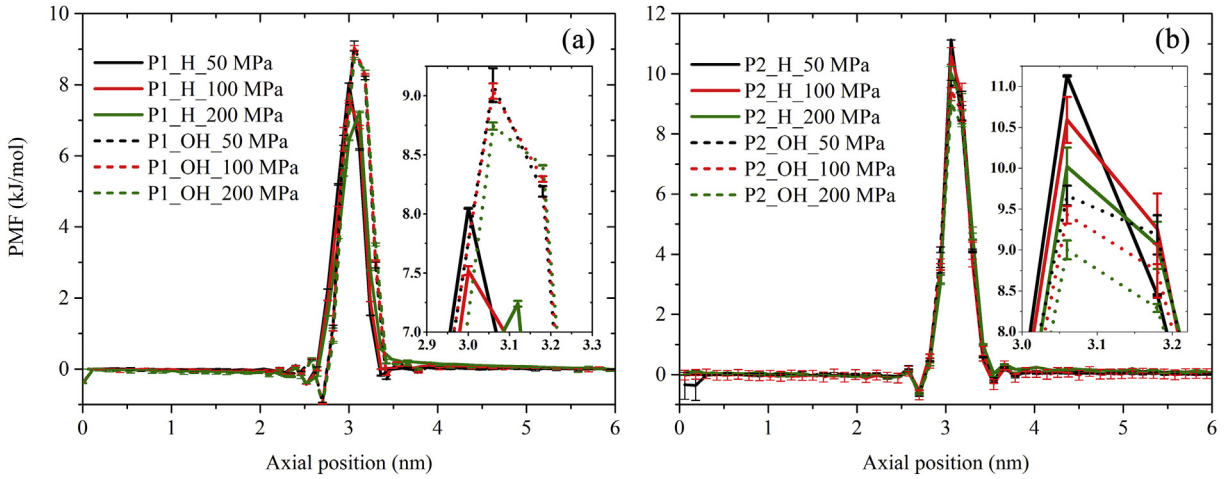

Fig. 7. PMF of water for (a) P1_H and P1_OH, (b) P2_H and P2_OH pores at the pressure of 50, 100 and 200 MPa in the time stage of 29–30 ns. (A colour version of this figure can be viewed online.)

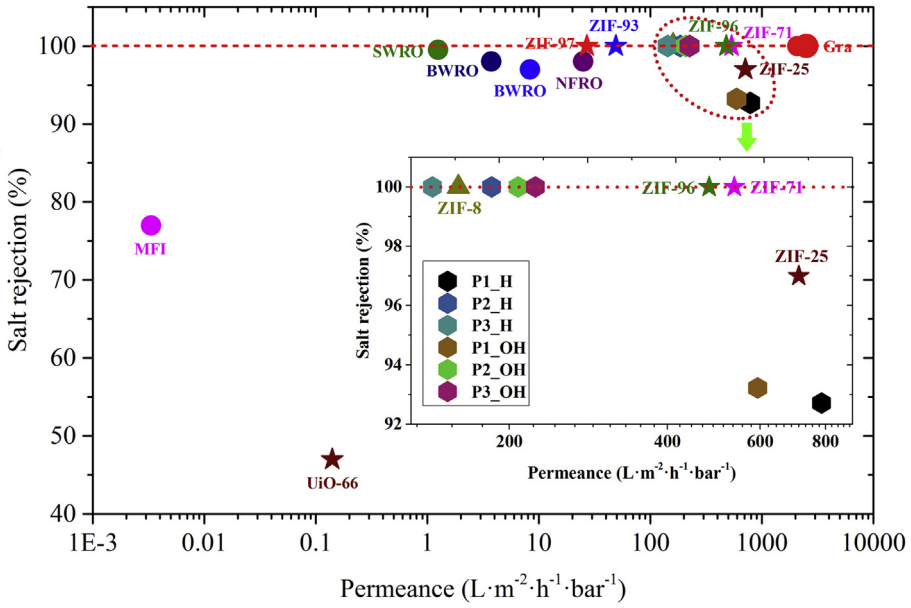

Fig. 8. Performance chart for functionalized nanoporous graphene (for P1, P2 and P3 pores) versus existing technologies. (A colour version of this figure can be viewed online.)

through. The energy barrier for water molecule passing over the membrane increases with the decreasing of pore size. Therefore, the N_w and water flux decreasing in the order of P1 < P2 < P3 in Figs. 3 and 4 for both hydrogenated and hydroxylated membranes can be explained. Generally, it can be seen that there are different infiltration performances between P1 and P2 and the same performances between the P2 and P3 regarding the hydrogen and hydroxyl groups. Herein, the calculated PMFs for P1 and P2 pore membranes under the induced pressures of 50, 100 and 200 MPa are plotted in Fig. 7. From the inset of Fig. 7(a), we can see that the energy barriers of P1_OH are always larger than those of P1_H, however, the opposite trend can be observed in the inset of Fig. 7(b) and Fig. S3. In addition, the energy barrier will be decreased with the induced pressure increasing for the both P1 and P2 membranes. All the findings are consistent with the trends that demonstrated in Fig. 3.

From all above results, we demonstrated that our functionalized nanoporous graphene could act as a RO membrane by simultaneously allowing for water permeation (Fig. 3) and rejecting salt ions (Fig. 5). We also calculated the water permeance and estimated salt rejection for all the designed graphene membranes, and the results are plotted together with the experimental performance of RO in Fig. 8. Among the P1, P2 and P3 configurations that shown both high water permeance and salt rejection rate (per 878.5 Å^2 for both hydrogenated and hydroxylated for one pore), the water permeance is ranged from 82.3 to 785.6 L per m^2·h·bar. As a comparison, graphene membranes which we used have higher permeance than MFI zeolite [35], UiO-66 [38], seawater RO, Brackish RO, nanofiltration and high-flux RO [63]. Especially, P2 at low pressure and P3 membranes at all pressures show 100% salt rejection and a water permeance of 2–3 orders of magnitude higher than those of available RO membranes. However, the membranes in this work have a slightly lower permeance than ZIF-8 [37] and previously examined graphene [19], because of the lower pore density than the two latter membranes. This indicates that functionalized nanoporous graphene membrane has great potential for water desalination.

4. Conclusion

Herein, we have investigated nanoporous graphene membranes with three pore diameters which were further functionalized by hydrogen or hydroxyl groups for water desalination. Both water flux and salt rejection were found to be sensitive to the pore diameter and chemical functionalization. The water flux increases with increasing external pressure due to decrease in energy barrier of water molecules. With largest pore P1 among three pores, water flux is highest, however, sacrificing the salt rejection compared to smaller pores P2 and P3. More specifically, the Na^+ ions prefer to go through the P1_H membrane and Cl^- ions prefer to P1_OH membrane because of favorable electrostatic interactions of the functional groups. Moreover, both Na^+ and Cl^- ions cannot penetrate the P2 and P3 membranes. Furthermore, compared to existing technology, two or three orders of magnitude higher water permeance of 785.6 L per m^2·h·bar baris obtained. This simulation study reveals that functionalized graphene membrane might be a fascinating RO membrane material for water desalination.

Acknowledgements

This work was supported by NSF of China (Grant No. 21373113, 21506178), Fundamental Research Funds for the Central Universities No. 30920140111008, and A Project Funded by the Priority Academic Program Development of Jiangsu Higher Education Institutions (PAPD). We are grateful to the A*star of Singapore (R-279-000-431-305) and the National University of Singapore (R-279-000-437-112) for financial support. Y.H. Wang also acknowledges the support from the program of China Scholarship Council (CSC).

Appendix A. Supplementary data

Supplementary data related to this article can be found at http://dx.doi.org/10.1016/j.carbon.2017.01.099.

References

[1] J. Eliasson, The rising pressure of global water shortages, Nature 517 (7532) (2015) 6.
[2] M. Alamaro, Water politics must adapt to a warming world, Nature 514 (7520) (2014) 7.
[3] M.A. Shannon, P.W. Bohn, M. Elimelech, J.G. Georgiadis, B.J. Mariñas,

A.M. Mayes, Science and technology for water purification in the coming decades, Nature 452 (7185) (2008) 301–310.
[4] M. Elimelech, W. Phillip, The future of seawater desalination: energy, technology, and the environment, Science 333 (6043) (2011) 712–717.
[5] C. Packer, R. Hilborn, A. Mosser, B. Kissui, M. Borner, G. Hopcraft, et al., Ecological change, group territoriality, and population dynamics in Serengeti lions, Science 307 (5708) (2005) 390–393.
[6] C.J. Vörösmarty, P. Green, J. Salisbury, R.B. Lammers, Global water resources: vulnerability from climate change and population growth, Science 289 (5477) (2000) 284–288.
[7] L. Ruiz, Y. Wu, S. Keten, Tailoring the water structure and transport in nanotubes with tunable interiors, Nanoscale 7 (1) (2015) 121–132.
[8] K.W. Zhao, H.Y. Wu, Fast water thermo-pumping flow across nanotube membranes for desalination, Nano Lett. 15 (6) (2015) 3664–3668.
[9] R. Das, M.E. Ali, S.B.A. Hamid, S. Ramakrishna, Z.Z. Chowdhury, Carbon nanotube membrane for water purification: a bright future in water desalination, Desalination 336 (1) (2014) 97–109.
[10] Z.J. He, B. Corry, X.H. Lu, J. Zhou, A mechanical nano gate based on a carbon nanotube for reversible control of ion conduction, Nanoscale 6 (7) (2014) 3686–3694.
[11] M. Majumder, N. Chopra, R. Andrews, B.J. Hinds, Nanoscale hydrodynamics: enhanced flow in carbon nanotubes, Nature 438 (7064) (2005) 44.
[12] S. Kar, R.C. Bindal, P.K. Tewari, Carbon nanotube membranes for desalination and water purification: challenges and opportunities, Nano Today 7 (5) (2012) 385–389.
[13] S. Joseph, N.R. Aluru, Why are carbon nanotubes fast transporters of water? Nano Lett. 8 (2) (2008) 452–458.
[14] A. Alexiadis, S. Kassinos, Molecular simulation of water in carbon nanotubes, Chem. Rev. 108 (12) (2008) 5014–5034.
[15] Y. Ren, F. Li, H.M. Cheng, K. Liao, Tension-tension fatigue behavior of unidirectional single-walled carbon nanotube reinforced epoxy composite, Carbon 41 (11) (2003) 2177–2179.
[16] Y. Zhang, Z. Shi, Z. Gu, S. Iijima, Structure modification of single-wall carbon nanotubes, Carbon 38 (15) (2000) 2055–2059.
[17] S.W. Kim, T. Kim, Y.S. Kim, H.S. Choi, H.J. Lim, S.J. Yang, et al., Surface modifications for the effective dispersion of carbon nanotubes in solvents and polymers, Carbon 50 (1) (2012) 3–33.
[18] Z.J. He, J. Zhou, Probing carbon nanotube-amino acid interactions in aqueous solution with molecular dynamics simulations, Carbon 78 (78) (2014) 500–509.
[19] D. Cohen-Tanugi, J.C. Grossman, Water desalination across nanoporous graphene, Nano Lett. 12 (7) (2012) 3602–3608.
[20] D. Cohen-Tanugi, J.C. Grossman, Water permeability of nanoporous graphene at realistic pressures for reverse osmosis desalination, J. Chem. Phys. 141 (7) (2012) 074704.
[21] Z.J. He, J. Zhou, X.H. Lu, B. Corry, Bioinspired graphene nano pores with voltage-tunable ion selectivity for Na^+ and K^+, ACS Nano 7 (11) (2013) 10148–10157.
[22] D. Konatham, J. Yu, T.A. Ho, A. Striolo, Simulation insights for graphene-based water desalination membranes, Langmuir 29 (38) (2013) 11884–11897.
[23] K. Celebi, J. Buchheim, R.M. Wyss, A. Droudian, P. Gasser, I. Shorubalko, et al., Ultimate permeation across atomically thin porous graphene, Science 344 (6181) (2014) 289–292.
[24] G.P. Liu, W.Q. Jin, N.P. Xu, Graphene-based membrane, Chem. Soc. Rev. 44 (15) (2015) 5016–5030.
[25] Z.G. Song, Z.P. Xu, Ultimate osmosis engineered by the pore geometry and functionalization of carbon nanostructures, Sci. Rep. 5 (2015) 10597.
[26] Q. Chen, X.N. Yang, Pyridinic nitrogen doped nanoporous graphene as desalination membrane: molecular simulation study, J. Membr. Sci. 496 (2015) 108–117.
[27] T.A. Ho, A. Striolo, Promising performance indicators for water desalination and aqueous capacitors obtained by engineering the electric double layer in nano structured carbon electrodes, J. Phys. Chem. C 119 (6) (2015) 3331–3337.
[28] D. Cohen-Tanugi, J.C. Grossman, Nanoporous graphene as a reverse osmosis membrane: recent insights from theory and simulation, Desalination 366 (2015) 59–70.
[29] D.Y. Koh, R.P. Lively, Nanoporous graphene: membranes at the limit, Nat. Nanotechnol. 10 (5) (2015) 385–386.
[30] S.P. Surwade, S.N. Smirnov, I.V. Vlassiouk, R.R. Unocic, G.M. Veith, S. Dai, et al., Water desalination using nanoporous single-layer graphene, Nat. Nanotechnol. 10 (5) (2015) 459–464.
[31] P.S. Goh, A.F. Ismail, Graphene-based nano material: the state-of-the-art material for cutting edge desalination technology, Desalination 356 (2015) 115–128.
[32] P. Kuhn, M. Antonietti, A. Thomas, Porous, covalent triazine-based frameworks prepared by ionothermal synthesis, Angew. Chem. Int. Ed. 47 (18) (2008) 3450–3453.
[33] P. Katekomol, J. Roeser, M. Bojdys, J. Weber, A. Thomas, Covalent triazine frameworks prepared from 1, 3, 5-tricyanobenzene, Chem. Mater. 25 (9) (2013) 1542–1548.
[34] L.C. Lin, J. Cho, J.C. Grossman, Two-dimensional covalent triazine framework as an ultrathin-film nanoporous membrane for desalination, Chem. Commun. 51 (80) (2015) 14921–14924.
[35] M.M. Pendergast, E.M.V. Hoek, A review of water treatment membrane nanotechnologies, Energy Environ. Sci. 4 (6) (2011) 1946–1971.
[36] Z.Q. Hu, Y.F. Chen, J.W. Jiang, Zeolitic imidazolate framework-8 as a reverse osmosis membrane for water desalination: insight from molecular simulation, J. Chem. Phys. 134 (13) (2011) 134705.
[37] K.M. Gupta, K. Zhang, J.W. Jiang, Water desalination through zeolitic imidazolate framework membranes: significant role of functional groups, Langmuir 31 (48) (2015) 13230–13237.
[38] X.L. Liu, N.K. Demir, Z.T. Wu, K. Li, Highly water-stable zirconium metal–organic framework UiO-66 membranes supported on alumina hollow fibers for desalination, J. Am. Chem. Soc. 137 (22) (2015) 6999–7002.
[39] F. Fornasiero, J.B. In, S. Kim, H.G. Park, Y. Wang, C.P. Grigoropoulos, et al., pH-tunable ion selectivity in carbon nanotube pores, Langmuir 26 (18) (2010) 14848–14853.
[40] F. Fornasiero, H.G. Park, J.K. Holt, M. Stadermann, C.P. Grigoropoulos, A. Noy, et al., Ion exclusion by sub-2-nm carbon nanotube pores, Proc. Natl. Acad. Sci. U. S. A. 105 (45) (2008) 17250–17255.
[41] S. Bae, H. Kim, Y. Lee, X. Xu, J. Park, Y. Zheng, et al., Roll-to-roll production of 30-inch graphene films for transparent electrodes, Nat. Nanotechnol. 5 (8) (2010) 574–578.
[42] V. Berry, Impermeability of graphene and its applications, Carbon 62 (10) (2013) 1–10.
[43] J.S. Bunch, S.S. Verbridge, J.S. Alden, A.M. van der Zande, J.M. Parpia, H.G. Craighead, et al., Impermeable atomic membranes from graphene sheets, Nano Lett. 8 (8) (2008) 2458–2462.
[44] S.C. O'Hern, M.S.H. Boutilier, J. Idrobo, Y. Song, J. Kong, T. Laoui, et al., Selective ionic transport through tunable subnanometer pores in single-layer graphene membranes, Nano Lett. 14 (3) (2014) 1234–1241.
[45] H. Du, J. Li, J. Zhang, G. Su, X. Li, Y. Zhao, Separation of hydrogen and nitrogen gases with porous graphene membrane, J. Phys. Chem. C 115 (47) (2011) 23261–23266.
[46] D.E. Jiang, V.R. Cooper, S. Dai, Porous graphene as the ultimate membrane for gas separation, Nano Lett. 9 (12) (2009) 4019–4024.
[47] Liu GP. ShenJ, K. Huang, Z.Y. Chu, W.Q. Jin, N.P. Xu, Subnanometer two-dimensional graphene oxide channels for ultrafast gas sieving, ACS Nano 10 (3) (2016) 3398–3409.
[48] D.B. Li, W. Hu, J.Q. Zhang, H. Shi, Q. Chen, T.Y. Sun, et al., Separation of hydrogen gas from coal gas by graphene nanopores, J. Phys. Chem. C 119 (45) (2015) 25559–25565.
[49] K.J. Berean, J.Z. Ou, M. Nour, M.R. Field, M.M.Y.A. Alsaif, Y.C. Wang, et al., Enhanced gas permeation through graphene nanocomposites, J. Phys. Chem. C 119 (24) (2015) 13700–13712.
[50] A. Ambrosetti, P.L. Silvestrelli, Gas separation in nanoporous graphene from first principle calculations, J. Phys. Chem. C 118 (33) (2014) 19172–19179.
[51] Y.H. Tao, Q.Z. Xue, Z.L. Liu, M.X. Shan, C.C. Ling, T.T. Wu, et al., Tunable hydrogen separation in porous graphene membrane: first-principle and molecular dynamic simulation, ACS Appl. Mater. Interfaces 6 (11) (2014) 8048–8058.
[52] T.T. Wu, Q.Z. Xue, C.C. Ling, M.X. Shan, Y.H. Liu ZL.Tao, et al., Fluorine-modified porous graphene as membrane for CO_2/N_2 separation: molecular dynamic and first-principles simulations, J. Phys. Chem. C 118 (14) (2014) 7369–7376.
[53] L.W. Drahushuk, M.S. Strano, Mechanisms of gas permeation through single layer graphene membranes, Langmuir 28 (48) (2012) 16671–16678.
[54] H.L. Du, J.Y. Li, J. Zhang, G. Su, X.Y. Li, Y.L. Zhao, Separation of hydrogen and nitrogen gases with porous graphene membrane, J. Phys. Chem. C 115 (47) (2011) 23261–23266.
[55] J. Schrier, Fluorinated and nanoporous graphene materials as sorbents for gas separations, ACS Appl. Mater. Interfaces 3 (11) (2011) 4451–4458.
[56] J. Schrier, Helium separation using porous graphene membranes, J. Phys. Chem. Lett. 1 (15) (2010) 2284–2287.
[57] S. Garaj, S. Liu, J.A. Golovchenko, D. Branton, Molecule-hugging graphene nanopores, Proc. Natl. Acad. Sci. U. S. A. 110 (30) (2013) 12192–12196.
[58] J. Prasongkit, A. Grigoriev, B. Pathak, R. Ahuja, ScheicherRH. Theoretical study of electronic transport through DNA nucleotides in a double-functionalized graphene nano gap, J. Phys. Chem. C 117 (29) (2013) 15421–15428.
[59] H. Jeong, H.S. Kim, S.H. Lee, D. Lee, Y.H. Kim, N. Huh, Quantum interference in DNA bases probed by graphene nanoribbons, Appl. Phys. Lett. 103 (103) (2013) 023701.
[60] C. Sathe, X.Q. Zou, J.P. Leburton, K. Schulten, Computational investigation of DNA detection using graphene nanopores, ACS Nano 5 (11) (2011) 8842–8851.
[61] D.B. Wells, M. Belkin, J. Comer, A. Aksimentiev, Assessing graphene nanopores for sequencing DNA, Nano Lett. 12 (8) (2012) 4117–4123.
[62] T. Kuila, S. Bose, A.K. Mishra, P. Khanra, N.H. Kim, J.H. Lee, Chemical functionalization of graphene and its applications, Prog. Mater. Sci. 57 (7) (2012) 1061–1105.
[63] G. Guillen, E.M.V. Hoek, Modeling the impacts of feed spacer geometry on reverse osmosis and nanofiltration processes, Chem. Eng. J. 149 (1–3) (2009) 221–231.
[64] A.K. Soper, F. Bruni, M.A. Ricci, Site-site pair correlation functions of water from 25 to 400°C: revised analysis of new and old diffraction data, J. Chem. Phys. 106 (1) (1997) 247–254.
[65] Z. He, J. Zhou, X. Lu, B. Corry, Ice-like water structure in carbon nanotube (8,8) induces cationic hydration enhancement, J. Phys. Chem. C 117 (21) (2013) 11412–11420.
[66] B. Hess, C. Kutzner, D. van der Spoel, E. Lindahl, GROMACS 4: algorithms for

highly efficient, load-balanced, and scalable molecular simulation, J. Chem. Theory Comput. 4 (3) (2008) 435–447.
[67] F. Zhu, E. Tajkhorshid, K. Schulten, Pressure-induced water transport in membrane channels studied by molecular dynamics, Biophys. J. 83 (1) (2002) 154–160.
[68] K.P. Travis, K.E. Gubbins, Poiseuille flow of Lennard-Jones fluids in narrow slit pores, J. Chem. Phys. 112 (4) (2000) 1984–1994.
[69] S. Bernardi, B.D. Todd, D.J. Searles, Thermostating highly confined fluids, J. Chem. Phys. 132 (24) (2010) 36–43.
[70] J. Muscatello, F. Jaeger, O.K. Matar, E.A. Müller, Optimizing water transport through graphene-based membranes: insights from nonequilibrium molecular dynamics, ACS Appl. Mater Interfaces 8 (19) (2016) 12330–12336.
[71] H. Frentrup, C. Avendaño, M. Horsch, A. Salih, E.A. Müller, Transport diffusivities of fluids in nanopores by nonequilibrium molecular dynamics simulation, Mol. Simul. 38 (7) (2012) 540–553.
[72] C. Huang, P.Y. Choi, L.W. Kostiuk, A method for creating a non-equilibrium NT (P1-P2) ensemble in molecular dynamics simulation, Phys. Chem. Chem. Phys. 13 (46) (2011) 20750–20759.
[73] M.E. Suk, N.R. Aluru, Molecular and continuum hydrodynamics in graphene nanopores, RSC Adv. 3 (24) (2013) 9365–9372.
[74] B. Corry, Designing carbon nanotube membranes for efficient water desalination, J. Phys. Chem. B 112 (5) (2008) 1427–1434.
[75] J. Azamat, A. Khataee, S.W. Joo, Molecular dynamics simulation of trihalomethanes separation from water by functionalized nanoporous graphene under induced pressure, Chem. Eng. Sci. 127 (2015) 285–292.
[76] R. Richard, S. Anthony, G. Aziz, Pressure-driven molecular dynamics simulations of water transport through a hydrophilic nanochannel, Mol. Phys. 114 (18) (2016) 2655–2663.
[77] W.L. Jorgensen, J. Chandrasekhar, J.D. Madura, R.W. Impey, M.L. Klein, Comparison of simple potential functions for simulating liquid water, J. Chem. Phys. 79 (2) (1983) 926–935.
[78] A.D. MacKerell, D. Bashford, M. Bellott, R.L. Dunbrack, J.D. Evanseck, M.J. Field, et al., All-atom empirical potential for molecular modeling and dynamics studies of proteins, J. Phys. Chem. B 102 (18) (1998) 3586–3616.
[79] G. Hummer, J.C. Rasaiah, J.P. Noworyta, Water conduction through the hydrophobic channel of a carbon nanotube, Nature 414 (6860) (2001) 188–190.
[80] J.L. Kou, X.Y. Zhou, H.J. Lu, F.M. Wu, J.T. Fan, Graphyne as the membrane for water desalination, Nanoscale 6 (3) (2014) 1865–1870.
[81] K. Sint, B. Wang, P. Kral, Selective ion passage through functionalized graphene nanopores, J. Am. Chem. Soc. 130 (49) (2008) 16448–16449.
[82] D. Cohen-Tanugi, L.C. Lin, J.C. Grossman, Multilayer nanoporous graphene membranes for water desalination, Nano Lett. 16 (2) (2016) 1027–1033.
[83] L.L. Zhang, G. Wu, J.W. Jiang, Adsorption and diffusion of CO2 and CH4 in zeolitic imidazolate framework-8: effect of structural flexibility, J. Phys. Chem. C 118 (17) (2014) 8788–8794.
[84] B. Roux, The calculation of the potential of mean force using computer-simulations, Comput. Phys. Commun. 91 (1–3) (1995) 275–282.